Mon. Not. R. Astron. Soc. **330,** 685–698 (2002)

Evolution of a 3-$M_\odot$ star from the main sequence to the ZZ Ceti stage: the role played by element diffusion

L. G. Althaus,★† A. M. Serenelli,★‡ A. H. Córsico★‡ and O. G. Benvenuto★§
Facultad de Ciencias Astronómicas y Geofísicas, Universidad Nacional de La Plata, Paseo del Bosque S/N, (1900) La Plata, Argentina

Accepted 2001 October 26. Received 2001 October 26; in original form 2001 August 22

ABSTRACT

The purpose of this paper is to present new full evolutionary calculations for DA white dwarf stars with the major aim of providing a physically sound reference frame for exploring the pulsation properties of the resulting models in future communications. Here, white dwarf evolution is followed in a self-consistent way with the predictions of time-dependent element diffusion and nuclear burning. In addition, full account is taken of the evolutionary stages prior to white dwarf formation. In particular, we follow the evolution of a 3-$M_\odot$ model from the zero-age main sequence (the adopted metallicity is $Z = 0.02$), all the way from the stages of hydrogen and helium burning in the core up to the thermally pulsing phase. After experiencing 11 thermal pulses, the model is forced to evolve towards its white dwarf configuration by invoking strong mass loss episodes. Further evolution is followed down to the domain of the ZZ Ceti stars on the white dwarf cooling branch.

Emphasis is placed on the evolution of the chemical abundance distribution caused by diffusion processes and the role played by hydrogen burning during the white dwarf evolution. We find that discontinuities in the abundance distribution at the start of the cooling branch are considerably smoothed out by diffusion processes by the time the ZZ Ceti domain is reached. Nuclear burning during the white dwarf stage does not represent a major source of energy, as expected for a progenitor star of initially high metallicity. We also find that thermal diffusion lessens even further the importance of nuclear burning.

Furthermore, the implications of our evolutionary models for the main quantities relevant for adiabatic pulsation analysis are discussed. Interestingly, the shape of the Ledoux term is markedly smoother compared with previous detailed studies of white dwarfs. This is translated into a different behaviour of the Brunt–Väisälä frequency.

Key words: stars: evolution – stars: interiors – stars: oscillations – white dwarfs.

1 INTRODUCTION

Over the last few years, radial and particularly non-radial stellar pulsations have become a very powerful tool for enquiring into the internal structure and evolution of stars. Thanks to the increasing degree of sophistication both in theoretical and observational techniques, asteroseismology has been successfully applied to deciphering the oscillatory pattern of numerous pulsating stars, amongst which our Sun represents the best example. With the advancement and refinement of observations, a large number of stellar objects located in a variety of places in the Hertzsprung–Russell diagram has gradually manifested themselves in non-radial pulsators. Indeed, variable stars covering several evolutionary stages, such as roAp, SPB, δ Scuti, β Cephei and variable white dwarfs have been classified as non-radial pulsators (see, for example, Cox 1980; Unno et al. 1989; Brown & Gilliland 1994; Gaustchy & Saio 1995, 1996). To this class also belong the recently discovered sdB (Kilkenny et al. 1997) and γ Doradus (Kaye et al. 1999) variable stars.

From the observational point of view (with the obvious exception of our Sun), white dwarfs represent one of the best established and most extensively studied kind of non-radial pulsators. Pulsating white dwarfs exhibits multiperiodic luminosity variations in three different regions of the Hertzsprung–Russell

★E-mail: althaus@fcaglp.fcaglp.unlp.edu.ar (LGA); serenell@fcaglp.fcaglp.unlp.edu.ar (AMS); acorsico@fcaglp.fcaglp.unlp.edu.ar (AHC); obenvenu@fcaglp.fcaglp.unlp.edu.ar (OGB)
† Member of the Carrera del Investigador Científico y Tecnológico, Consejo Nacional de Investigaciones Científicas y Técnicas (CONICET), Argentina.
‡ Fellow of CONICET, Argentina.
§ Member of the Carrera del Investigador Científico, Comisión de Investigaciones Científicas de la Provincia de Buenos Aires, Argentina.

diagram corresponding to the currently called DOV (and PNNV), DBV and DAV (see, for example, the review by Winget 1988). Of particular interest in this work are the DAVs (with hydrogen-rich atmospheres), or ZZ Ceti stars, that are found to pulsate in the instability strip corresponding to the effective temperature ($T_{\rm eff}$) range of $12500 \geq T_{\rm eff} \geq 10700$ K. The periodicities in their light curves are basically explained in terms of non-radial g-modes of low harmonic degree ($\ell \leq 2$), driven by the $\kappa-\gamma$ mechanism working in a partial ionization region below the stellar surface (Dolez & Vauclair 1981; Winget et al. 1982).[1] The periods are found to be within a range of 100–1200 s and photometric amplitudes reach up to 0.30 mag. Numerous studies have been devoted to analysing the pulsation characteristics of DAV white dwarfs. Amongst them, we mention the works by Tassoul, Fontaine & Winget (1990), Brassard et al. (1991, 1992a,b), Bradley & Winget (1994), Gautschy, Ludwig & Freytag (1996) and Bradley (1996, 1998, 2001).

In order to fully understand the oscillatory properties of DAV white dwarfs and to take full advantage of the richness offered by available observations, physically sound stellar models are required. In the context of these pulsating stars, most of the existing research rests on stellar models constructed under the assumptions of some simplifying hypothesis. This is particularly true with regard to the treatment of the chemical abundance distribution. In this sense, carbon and oxygen profiles are usually treated as free parameters. In addition, the chemical abundance distribution is assumed to be fixed during the evolution across the instability domain and in some cases the diffusive equilibrium approximation is invoked to assess the shape of the chemical profile at the interface regions. Hydrogen burning is likewise neglected in the construction of evolutionary models employed in pulsation studies of ZZ Ceti stars. The neglect of hydrogen burning is only justified if the white dwarf is formed with relatively thin hydrogen layers. However, if the hydrogen envelope is massive enough, hydrogen burning reactions constitute an appreciable source of energy even during the evolutionary stages corresponding to the ZZ Ceti domain (Iben & Tutukov 1984). The details of burning are more complex if element diffusion is allowed to operate. Indeed, white dwarf evolutionary calculations in which time-dependent element diffusion is properly accounted for (Iben & MacDonald 1986) show that nuclear burning via the CN reactions plays a different role depending on the mass of the helium buffer region between the hydrogen-rich envelope and the carbon- and helium-rich underlying layers. For instance, a diffusion-induced hydrogen shell flash is expected to occur if the helium buffer is sufficiently less massive. How massive the helium buffer can be depends critically on the phase in the helium shell flash cycle during the thermally pulsing stage at which the progenitor departs from the asymptotic giant branch (AGB) (see D'Antona & Mazzitelli 1990 for details).

Obviously, the construction of stellar models of DAV white dwarfs appropriate for pulsation studies in which the above-mentioned issues are fully taken into account requires evolutionary calculations considering not only time-dependent element diffusion but also a detailed treatment of the evolutionary stages prior to white dwarf formation. The calculation of such stellar models is the main purpose of the present work and to the best of our knowledge such an endeavour has never been attempted. The primary application of the DA white dwarf evolutionary models to be presented here will be the exploration of their pulsation properties in future papers. Specifically, in this paper we shall limit ourselves to discussing the evolutionary results and their implications for the main quantities entering the adiabatic pulsation equations.

White dwarf evolution treated in a self-consistent way with time-dependent element diffusion is an important aspect of the present work. In most of previous pulsation studies, the equilibrium diffusion in the trace element approximation has been used to specify the shape of the chemical profile at the composition transition region of evolving stellar models (see Tassoul et al. 1990; Brassard et al. 1991, 1992a,b; Bradley 1996, 1998, 2001; Bradley & Winget 1994; Montgomery, Metcalfe & Winget 2001). However, the equilibrium approach for diffusion is not valid when diffusion time-scales are comparable to the evolutionary ones. In particular, diffusive equilibrium in the deep layers of the white dwarf model is not an adequate approximation even at the ages characteristic of the ZZ Ceti stage. In fact, it is found that during such stages, diffusion modifies the spatial distribution of the elements, particularly at the chemical interfaces (see Iben & MacDonald 1985). For a proper treatment of the diffusively evolving stratifications, we consider in this work the processes of gravitational settling, chemical and thermal diffusion following the treatment of Burgers (1969) for multicomponent gases. In the context of DA white dwarf evolution, the treatment for diffusion we shall use here has been employed by Iben & MacDonald (1985, 1986). In addition, Dehner & Kawaler (1995) have used non-equilibrium diffusion star models for studying the connection between DO and DB white dwarfs. The shape of the composition transition zone is a matter of the utmost importance as far as asteroseismology is concerned. In particular, it contributes to the shape of the Ledoux term appearing in the Brunt–Väisälä frequency (Brassard et al. 1991) and plays a critical role in the phenomenon of mode trapping in white dwarfs (see Tassoul et al. 1990; Brassard et al. 1992a and references cited therein).

Another important aspect of the present study is that the evolutionary stages prior to the white dwarf formation are fully taken into account. Specifically, we started our calculations from a 3-$M_{\odot}$ stellar model at the zero-age main sequence (ZAMS) and we follow its further evolution all the way from the stage of hydrogen and helium burning in the core up to the tip of the AGB where helium thermal pulses occur. To ensure full relaxation of the helium zone (see Mazzitelli & D'Antona 1986), we computed a reasonable number of thermal pulses, after which the progenitor is forced to evolve towards its white dwarf configuration by invoking strong mass loss episodes. We shall concentrate on the particular situation where the white dwarf progenitor departs from the AGB when stationary helium burning primarily supports the star luminosity, following the occurrence of the last helium thermal pulse. We have not invoked additional mass losses during the planetary nebula stage or early during the cooling branch. This will allow us to examine the maximum mass value for the remaining hydrogen content as predicted by the particular case of evolution analysed in this work, enabling us to explore the role played by nuclear burning during the cooling stages.

The paper is organized as follows. In Section 2 we describe our evolutionary code and the treatment we follow for element diffusion. In Section 3 we present in detail the evolutionary results for the white dwarf progenitor, giving particular emphasis to the thermal micropulses appearing towards the end of core helium burning and the thermally pulsing phase during the final AGB

[1] However, Brickhill (1991) proposed the convective driving mechanism as being responsible for the overstability of g-modes in DAVs (see also Goldreich & Wu 1999).

evolution. In this section, we also present the results for the post-AGB and white dwarf evolution. Attention is focused mainly on the evolution of the chemical distribution resulting from diffusion processes and the role of nuclear burning during the white dwarf regime. The implications of the evolutionary results for the main quantities relevant for adiabatic pulsation analysis are detailed in Section 4. Finally, Section 5 is devoted to summarizing our results.

2 COMPUTATIONAL DETAILS

The calculations presented in this work have been performed with the stellar evolutionary code developed at La Plata Observatory. The code has been used in our previous studies on white dwarf evolution (Althaus & Benvenuto 1997, 2000; Benvenuto & Althaus 1998), and it has recently been appropriately modified in order to calculate the evolutionary stages prior to the formation of white dwarfs. In broad outline, the code is based on the method of Kippenhahn, Weigert & Hofmeister (1967) for calculating stellar evolution. In particular, to specify the outer boundary conditions we carried out three envelope integrations from photospheric starting values inward to a fitting outer mass fraction, which is located in mass near the photosphere. The interior solution is obtained via the canonical Henyey iteration scheme as described by Kippenhahn et al. (1967). To improve the numerical stability of our code, the Henyey scheme is applied to the differences in the physical quantities (luminosity, pressure, radius and temperature) between the previous and the computed models. In addition, models were divided into approximately 1500 mesh points and time-steps were maintained small enough so as to obtain a reasonable numerical accuracy during the thermal pulses at the tip of the AGB. The mesh distribution is regularly updated every five time-steps. Our algorithm inserts mesh points where they are most needed, that is where physical variables change appreciably, and eliminates them where they are not necessary. We want to mention that the entire evolutionary sequence from the ZAMS to the white dwarf stage comprises $\sim$60 000 stellar models.

The constitutive physics are as detailed and updated as possible. Briefly, it comprises OPAL radiative opacities (including carbon- and oxygen-rich opacities) for arbitrary metallicities (Iglesias & Rogers 1996), complemented at low temperatures with the molecular opacities from Alexander & Ferguson (1994). In particular, opacities for varying metallicities are required during the white dwarf regime when account is taken in the calculations of element diffusion. The conductive opacity for the high-density regime is taken from Itoh et al. (1983) and Hubbard & Lampe (1969) for low densities. Neutrino emission rates for pair, photo, plasma and bremsstrahlung processes have been taken into account according to the formulation of Itoh and collaborators (see Althaus & Benvenuto 1997 for details). As far as the equation of state is concerned, we have included partial ionization, radiation pressure, ionic contributions, partially degenerate electrons and Coulomb interactions. For the white dwarf regime, we employ an updated version of the equation of state of Magni & Mazzitelli (1979). We have considered a network of 30 thermonuclear reaction rates for hydrogen burning (corresponding to the proton–proton chain and the CNO bi-cycle) and helium burning. Nuclear reaction rates are taken from Caughlan & Fowler (1988) except for the reaction $^{12}C(\alpha,\gamma)^{16}O$ which is taken from Angulo et al. (1999) [this rate is approximately twice as large as that of Caughlan & Fowler (1988)]. Electron screening is taken from Graboske et al. (1973) and Wallace, Woosley & Weaver (1982). The change in the chemical composition resulting from nuclear burning is computed by means of a standard implicit method of integration. In particular, we follow the evolution of the chemical species ^{1}H, ^{3}He, ^{4}He, ^{7}Li, ^{7}Be, ^{12}C, ^{13}C, ^{14}N, ^{15}N, ^{16}O, ^{17}O, ^{18}O and ^{19}F. Convection has been treated following the standard mixing length theory (Böhm-Vitense 1958) with mixing-length to pressure scaleheight $\alpha = 1.5$. The Schwarzschild criterion was used to determine the boundaries of convective regions. Overshooting and semiconvection were not considered.

In this work, we follow the evolution of an initially 3-$M_\odot$ star starting at the ZAMS. The adopted metallicity Z is $Z = 0.02$ and the initial abundances by mass of hydrogen and helium are, respectively, $X_H = 0.705$ and $X_{He} = 0.275$ [representative for solar values as given by Anders & Grevesse (1989)]. Evolution has been computed at constant stellar mass all the way from the stages of hydrogen and helium burning in the core up to the tip of the AGB where helium thermal pulses occur. To achieve a white dwarf configuration, an artificial mass loss has been incorporated in our evolutionary code. Specifically, mass loss was initiated when the white dwarf progenitor was about to experience its 11th thermal pulse. The adopted mass loss rate was $10^{-4}\,M_\odot\,yr^{-1}$ and it was applied to each stellar model as evolution proceeded. After the convergence of each new stellar model, the total stellar mass is reduced according to the time-step used for the model and the mesh points are adjusted appropriately. We want to mention that because of the high computational demands involved in the calculation we perform here, particularly regarding the treatment of white dwarf evolution with diffusively evolving abundances (see below), we shall restrict ourselves exclusively to examining one case of evolution for the white dwarf progenitor, deferring a more detailed exploration of different possibilities of white dwarf formation to future works.

The evolution of the chemical abundance distribution caused by diffusion processes during the whole white dwarf stage represents an important aspect of the present study. In our treatment of element diffusion we have considered gravitational settling, and chemical and thermal diffusion of nuclear species. To this end, we adopted the treatment for multicomponent gases presented by Burgers (1969), avoiding the use of the trace element approximation usually assumed in white dwarf studies. It is worth noting that when the progenitor star departs from the AGB after the end of mass loss episodes, its envelope is made up of a mixture of hydrogen and helium. Also, in deeper layers and below the nearly pure helium buffer, there is an underlying region rich in both helium and carbon (see the next section); thus the use of the trace element approximation would not be appropriate for our purposes. In this study we are interested in the chemical evolution occurring quite deep in the star, thus radiative levitation and possible wind mass loss from the surface during the hot white dwarf stages, which are expected to alter the surface composition of these stars, have been neglected [see Unglaub & Bues (2000) for a recent detailed study of the evolution of chemical abundances in surface layers of hot white dwarfs]. In the context of white dwarf evolution, the treatment for diffusion we use here has been employed by Iben & MacDonald (1985, 1986)(thermal diffusion not included). Recently, it was applied by MacDonald, Hernanz & José (1998) to address the problem of carbon dredge-up in white dwarfs with helium-rich envelopes and by Althaus, Serenelli & Benvenuto (2001a,b) to explore the role played by diffusion in inducing thermonuclear flashes in low-mass, helium-core white dwarfs.

Details concerning the procedure we follow to solve the diffusion equations are given in Althaus & Benvenuto (2000). In

particular, we follow the evolution of the isotopes ^{1}H, ^{3}He, ^{4}He, ^{12}C, ^{14}N and ^{16}O. In order to calculate the dependence of the structure of our white dwarf models on the diffusively evolving abundances self-consistently, the set of equations describing diffusion has been coupled to our evolutionary code. After computing the change of abundances by effect of diffusion, they are evolved according to the requirements of nuclear reactions and convective mixing. Finally, we emphasize that radiative opacities during the white dwarf regime are calculated for metallicities consistent with the diffusion predictions. In particular, the metallicity is taken as twice the abundances of CNO elements as suggested by Iben & MacDonald (1986).

3 EVOLUTIONARY RESULTS

3.1 White dwarf progenitor

Here we describe the results we obtained with regard to the evolutionary phases prior to white dwarf formation. We shall limit ourselves to describing the main features of such evolution particularly those which are of immediate relevance for white dwarf formation, and we refer the reader to the works of Mazzitelli & D'Antona (1986), Vassiliadis & Wood (1993), Blöcker (1995a) amongst others for a more complete description concerning the evolution of low- and intermediate-mass stars. We begin by examining the complete evolutionary track in the Hertzsprung–Russell diagram that is illustrated in Fig. 1. Our numerical simulation covers all the evolutionary phases of an initially 3-$M_{\odot}$ star from the ZAMS to the domain of ZZ Ceti stars on the white dwarf cooling branch. The age (in units of 10^4 yr) from the end of mass loss episodes and the mass of hydrogen (in units of $10^{-4}\,M_{\odot}$) are indicated at selected points along the track. For clarity, the evolutionary phases corresponding to mass loss are not plotted.

After 4.1×10^8 yr of evolution and by the end of helium burning in the core, the first feature worthy of comment predicted by our calculations is the appearance of a series of micropulses (not to be confused with the major thermal pulses on the AGB) of low amplitude in the surface luminosity. Such micropulses are caused by thermal instabilities in the helium-burning shell above the carbon- and oxygen- rich core, which causes the helium luminosity to undergo oscillations. Specifically, such pulses appear when the central helium abundance by mass falls below $\approx$0.001 (and the convective core vanishes). The time dependence of the surface luminosity L_* and the helium-burning luminosity $L_{\rm He}$ (in solar units) during the micropulse phase is shown in two insets in Fig. 1, where the time-scale is given in Myr from the ZAMS. A total of 40

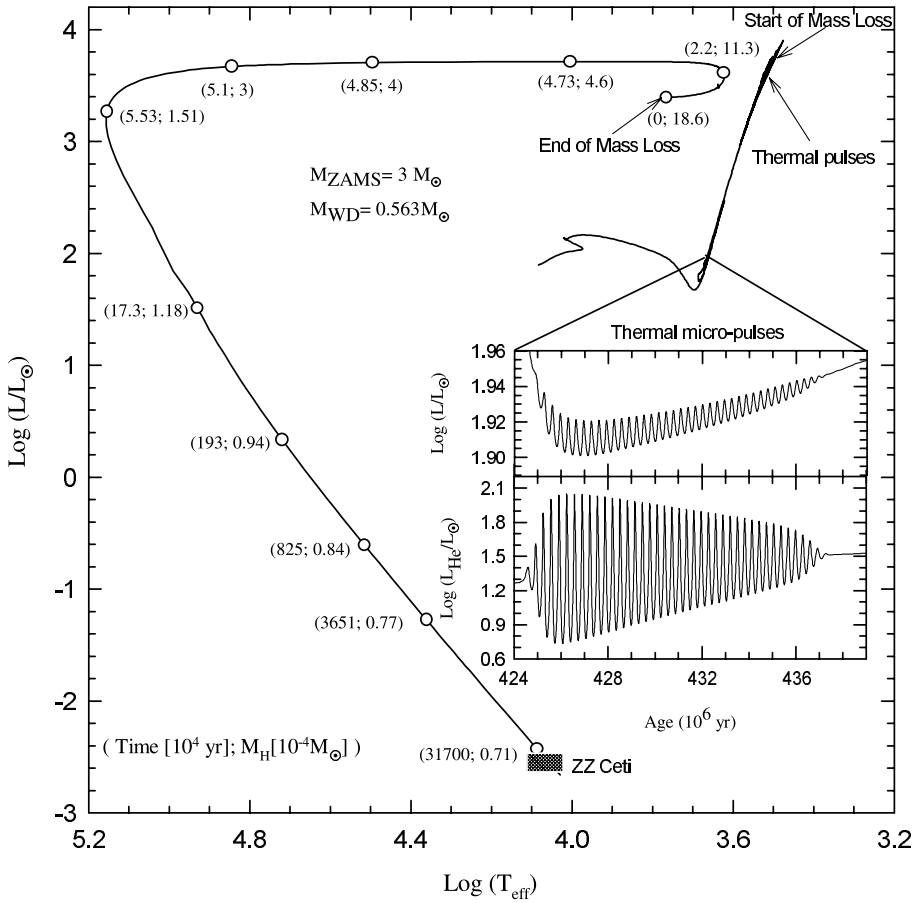

Figure 1. Hertzsprung–Russell diagram for the evolution of our 3-$M_{\odot}$ stellar model, from the ZAMS to the white dwarf stage. For clarity, the evolutionary stages corresponding to the mass loss phase are not shown. Numbers in parentheses besides circles along the track give the age (in 10^4 yr) measured from the end of mass loss and the mass of hydrogen in the outer layers in units of $10^{-4}\,M_{\odot}$. The domain of the ZZ Ceti instability strip is shown as a shaded region. As a result of mass loss episodes, the stellar mass decreases from 3 to 0.563 $M_{\odot}$. Note that after the end of mass loss, the star returns towards lower effective temperatures where it burns an appreciable fraction of its hydrogen content. During this phase, evolution proceeds very slowly. The inset displays the evolution of surface (top panel) and helium-burning (bottom panel) luminosities expressed in solar units during the thermal micropulses phase towards the end of helium burning in the stellar core.

micropulses with an interpulse period of $\approx 3.1 \times 10^5$ yr occurred. Note that the pulse amplitude in the surface luminosity is indeed modest [$\Delta\log(L/L_\odot) \approx 0.02$ at most]. It is worth mentioning that thermal micropulses occurring in a 3-$M_\odot$ star towards the end of its core helium-burning phase have also been reported by Mazzitelli & D'Antona (1986). After the end of the micropulses, the star evolves until complete helium exhaustion at the centre. The total time spent during central helium burning amounts to $\sim 1.25 \times 10^8$ yr.

After helium is exhausted in the core, leaving a central oxygen abundance of 0.62 by mass, evolution proceeds towards the phase of the major thermal pulses on the AGB, at which point helium shell burning becomes unstable again. The AGB evolution of intermediate-mass stars is well known to be characterized by helium shell flashes during which the burning rate rises very steeply. In our simulation, the time elapsed from central helium exhaustion until the first thermal pulse is 2.6×10^7 yr, when the surface luminosity exceeds $\log(L/L_\odot) = 3.2$ for the first time in its evolution. After experiencing 11 thermal pulses and considerable mass loss, the mass of the hydrogen envelope is reduced so much that the star departs from the AGB and evolves towards large effective temperatures. This takes place when the star luminosity is supported by stationary helium burning. We will discuss the implications of this situation later in this section, for now suffice it to say that when mass loss ends, the remnant consumes a considerable fraction of its remaining hydrogen in a redward 'hook' on the Hertzsprung–Russell diagram. During this phase, evolution proceeds very slowly.[2] As a result of mass loss episodes, the stellar mass has decreased from 3 to 0.563 $M_\odot$. Eventually, the remnant reaches the white dwarf cooling branch. Thereafter, element diffusion alters the chemical abundance distribution within the star even at the lowest computed luminosity stages. During the white dwarf cooling phase, the coupled effects of hydrogen burning and element diffusion reduce the mass of hydrogen that is left in outer layers by almost a factor of 2.

The time dependence of the surface luminosity during the thermally pulsing phase is detailed in the upper panel of Fig. 2, where the time-scale is given in Myr counted from the ZAMS. A total of 11 thermal pulses have been computed before the white dwarf progenitor departs from the AGB. This phase of evolution has been studied in detail by numerous authors in the literature (Schönberner 1979; Iben 1982; Iben & Renzini 1983; Vassiliadis & Wood 1993 amongst others) and we refer the reader to those studies for details. Let us, however, mention the role played by various relevant luminosities by the time the star next evolves away from the AGB towards the white dwarf state. To this end, we show in the lower panel of Fig. 2 the evolution of the surface luminosity (L_*) and the hydrogen- and helium-burning luminosities (L_H and L_{He}, respectively) during and between the 10th and 11th pulses. Departure from the AGB could, in principle, occur at different stages during the interpulse.

Here, we will direct our attention to one particular situation: that in which the star leaves the AGB during the quiescent helium-burning phase following the 11th helium thermal pulse. Our simulation is thus representative of the possibility that departure from the AGB takes place early in the helium shell flash cycle. The consequence for the post-AGB evolution resulting from departure at different locations on the interpulse has been explored carefully by numerous investigators (amongst them Iben 1984; Wood & Faulkner 1986; Blöcker 1995b). Such studies show, for instance,

[2] We want to mention that we have not considered further mass loss after the star has reached $\log T_{\rm eff} = 3.8$ for the first time after leaving the AGB.

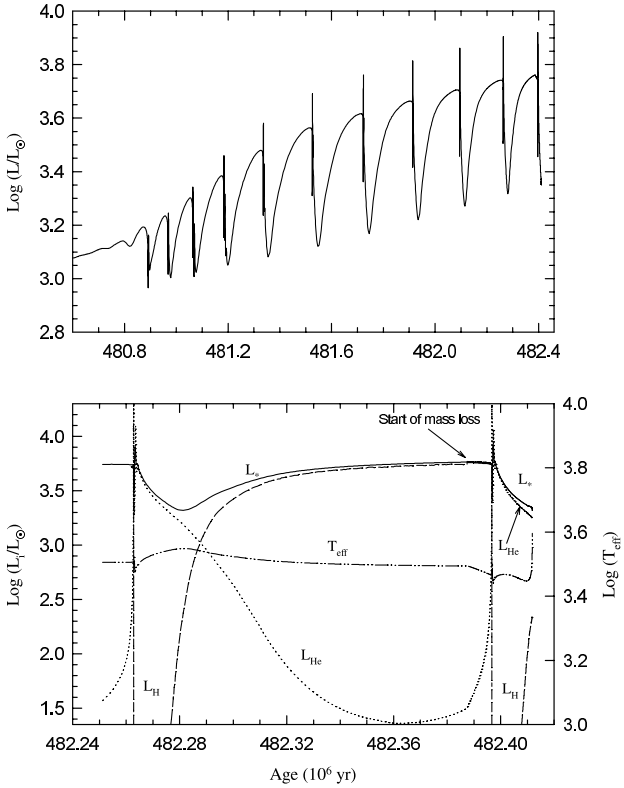

Figure 2. Top panel: evolution of surface luminosity (in solar units) during the phase corresponding to the helium thermal pulses for a 3-$M_\odot$ model at the top of the AGB. The model experiences a total of 11 pulses before departing from the AGB as a result of mass loss episodes. The time-scale is given in Myr from the ZAMS. Bottom panel: evolution of surface luminosity (L_*), helium-burning luminosity (L_{He}), hydrogen-burning luminosity (L_H) and effective temperature (T_{eff}) for the 3-$M_\odot$ model during and between its 10th and 11th thermal pulses. Note that the model departs from the AGB shortly after the occurrence of the 11th pulse peak when helium shell burning is dominant.

that the transition time from AGB to the planetary nebula region depends strongly on the phase at which the star leaves the AGB. From the bottom panel of Fig. 2 we see that the star departs from the AGB when helium shell burning is dominant. Specifically, the helium-burning shell contributes 82 per cent of the surface luminosity by the time the effective temperature begins to increase. In the meantime the hydrogen shell is almost extinguished. It is worth noting that the helium-burning luminosity in the shell source reaches $5 \times 10^6\,L_\odot$, causing an expansion in the layers above with the consequence that hydrogen burning decreases significantly to be almost extinguished and leading to a sharp spike in the surface luminosity. After that, the helium luminosity begins to drop and hydrogen is re-ignited.

For the sake of completeness, we show in Fig. 3 the behaviour of the central conditions during the whole evolution from the hydrogen burning in the core on the main sequence to the white dwarf state. Relevant episodes in the life of the star are indicated in the figure. In particular, the response of the central region to the occurrence of both thermal pulses and micropulses is noted. Once the remnant leaves the AGB, evolution proceeds at almost constant central density to become a white dwarf.

3.2 Post-AGB and white dwarf evolution

After the end of the thermally pulsing phase, the remnant star

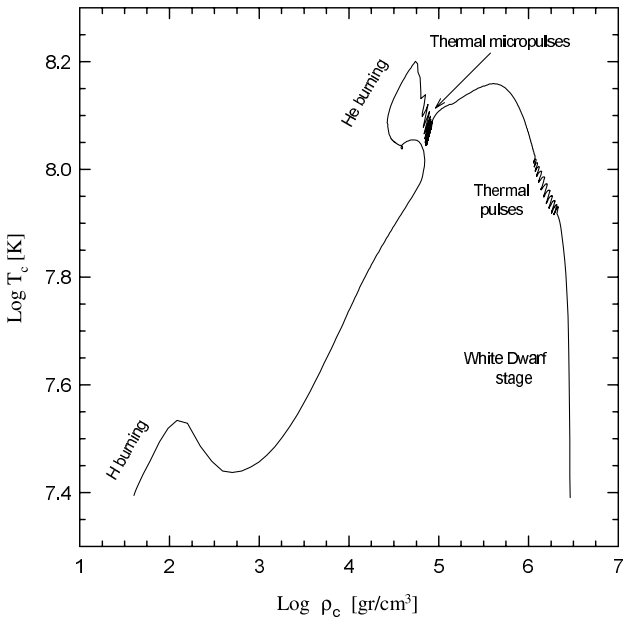

Figure 3. Central temperature versus central density corresponding to the evolution of the 3-$M_\odot$ model all the way from the ZAMS through the AGB towards the stage of white dwarf. Relevant episodes during the lifetime of the star such as hydrogen and helium burning, thermal micropulses and pulses are indicated as well.

departs from the asymptotic giant branch at low effective temperature and evolves as a planetary nebula nuclei towards higher effective temperatures. In Fig. 4 we show as a function of effective temperature the mass of hydrogen in outer layers (in units of $10^{-3}\,M_\odot$) for the 0.563-$M_\odot$ post-AGB remnant from a stage in the evolution just before the end of mass loss until that corresponding to the ZZ Ceti domain in the white dwarf regime. Numbers in parentheses besides circles at selected points on the curve give the age in years counted from the end of mass loss and the contribution of the helium shell burning to surface luminosity. By the end of mass loss (at $\log T_{\rm eff} = 3.8$) the contribution of the helium shell burning to surface luminosity has been reduced to 55 per cent. Thereafter, the remnant star returns to the AGB and increases its surface luminosity up to the interflash maximum value. During this phase, helium burning becomes less important and the hydrogen content in outer layers is reduced, as a result of increasing hydrogen burning, from $\approx 2\times10^{-3}\,M_\odot$ at the end of mass loss down to $\approx 5\times10^{-4}\,M_\odot$ once the remnant resumes its evolution to the blue. By the time the mass of the hydrogen content decreases below $\approx 8\times10^{-4}\,M_\odot$, helium burning becomes virtually extinct and hydrogen burning via the CN cycle reactions becomes the dominant source of surface luminosity. It is worth noting that evolution proceeds very slowly during this phase and the remnant star spends a substantial fraction of its post-AGB transition time there (~46 000 yr). Note also that the star takes ~48 000 yr to reach an effective temperature of 30 000 K required for the

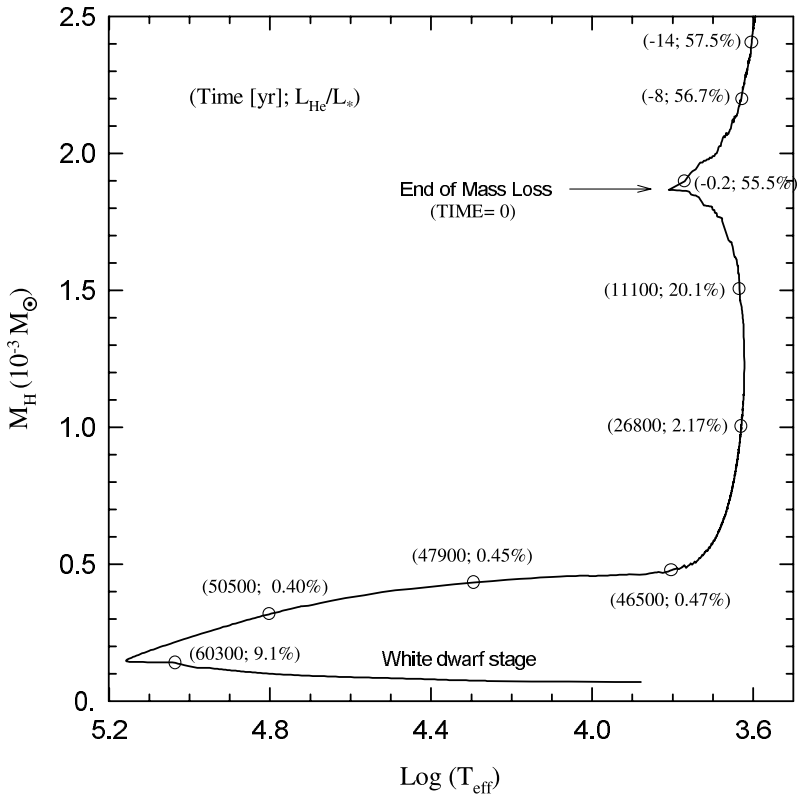

Figure 4. The mass of hydrogen in outer layers in units of 10^{-3} solar masses as a function of effective temperature for evolutionary stages following and immediately preceding the end of mass loss. The results correspond to a stellar remnant of $\approx 0.563\,M_\odot$ resulting from the evolution of a main-sequence progenitor of initially $3\,M_\odot$, which departed the AGB while helium shell burning dominates. Numbers in parentheses along the curve give the age (in yr) counted from the moment that mass loss is suppressed and the percentage contribution of helium burning to the surface luminosity. Note that when mass loss is halted, the star returns towards lower effective temperatures where, over a time interval of ≈40 000 yr, nuclear burning reduces the hydrogen mass by almost a factor of 4. Afterwards, the helium burning luminosity becomes negligible and the remnant resumes its evolution towards higher effective temperatures, eventually reaching the white dwarf stage with a hydrogen content of $\approx 1.5\times10^{-4}\,M_\odot$. Subsequent hydrogen burning reduces the residual hydrogen envelope mass by an additional factor of 2 before reaching the domain of the ZZ Ceti stars.

excitation of the planetary nebula. This time is so long that no planetary nebula is produced. These results resemble qualitatively those of Mazzitelli & D'Antona (1986), who found that if departure from the AGB takes place during the quiescent helium burning phase, then, when mass loss is stopped, the remnant spends a considerable time in consuming most of its hydrogen envelope as a red supergiant. Long post-AGB evolutionary time-scales were also found by Wood & Faulkner (1986) when their models are forced to abandon the AGB early in the interpulse phase. As well-known, post-AGB times are strongly dependent on the phase of the helium shell flash cycle at which the star leaves the AGB. In this regard, had our white dwarf progenitor been forced to depart from the AGB somewhat later than assumed here while burning hydrogen (by employing a smaller mass loss rate), it would not have returned to the AGB[3] and its further evolution would thus have proceeded much faster (see Mazzitelli & D'Antona 1986; Wood & Faulkner 1986). Note finally that the mass of hydrogen that is left in outer layers at the start of the cooling branch is $\sim 1.5 \times 10^{-4}\,M_\odot$, and this is reduced to $7 \times 10^{-5}\,M_\odot$ by the time the ZZ Ceti domain is reached. Because we have not invoked additional mass loss episodes during the planetary nebula stage or early during the cooling branch, the quoted value for the final hydrogen mass should be considered as an upper limit. We stress that in the present calculation we have adopted an initial metallicity of $Z = 0.02$; much lower values of Z would give rise to a larger final hydrogen envelope mass for the same stellar mass (see, for instance, Iben & MacDonald 1986).

Since the chemical stratification of the white dwarf is relevant for our purposes, let us detail the resulting chemical profile of the post-AGB remnant. In particular, the carbon and oxygen abundance distribution within the core of the remnant is detailed in Fig. 5. The inner part of the core of carbon and oxygen emerges from the convective helium core burning and from the subsequent stages in which the helium-burning shell propagates outwards. Note that this kind of profile is the typical one, apart from differences arising from the employment of different cross-sections for the $^{12}C + \alpha$ reaction rate, predicted by evolutionary models in which semiconvection and overshooting are not considered. The degree to which semiconvection and overshooting affect the core chemical stratification is an issue subject to debate and in most of studies in which this aspect is addressed, they are treated very roughly. Here we prefer not to include any of them in our models and this fact should be borne in mind by the reader. We simply want to mention that larger oxygen abundances are expected if convective overshooting brings fresh helium into the core during the final helium burning phases (see for instance Mazzitelli & D'Antona 1986 for more details). Before the remnant reaches its white dwarf configuration, a mixing episode occurs towards the central regions of the star. Indeed, we find that, as a result of the particular shape of the carbon–oxygen profile at $M_r/M_* \approx 0.2$, a Rayleigh–Taylor instability develops, which gives rise to a chemical rehomogenization of the innermost zone of the star (see Salaris et al. 1997 for a similar finding). The resulting carbon–oxygen distribution after rehomogenization, which is shown in Fig. 5 with thick lines, is the adopted one in this work for the remaining white dwarf evolution. Surrounding the carbon–oxygen interior there is a shell rich in both carbon (≈35 per cent) and helium (≈60 per cent), and an overlying layer consisting of nearly pure helium, the so-called helium buffer (see the inset in Fig. 5). The presence of carbon in the helium-rich region below the helium buffer stems from the short-lived convective mixing that has driven the carbon-rich zone upwards during the peak of the last helium pulse on the AGB. The mass of the helium buffer is of relevance in connection with the further evolution of the remnant during the white dwarf state, particularly regarding the occurrence of a hydrogen shell flash induced by element diffusion. In this regard, Iben & MacDonald (1986) have found that if the helium buffer mass is as small as $0.001\,M_\odot$, then a hydrogen shell flash is initiated as a result of chemical diffusion. In our simulation, when the progenitor departs from the AGB, the mass of the helium buffer is $3.4 \times 10^{-4}\,M_\odot$, but during the evolutionary phases in which the star, after the end of mass loss episodes, returns to the AGB to burn most of the remaining hydrogen content, the buffer mass increases up to $0.0024\,M_\odot$ (and to $0.003\,M_\odot$ at the white dwarf birth) as a result of nuclear burning at the base of the hydrogen envelope. The final helium buffer has thus become massive enough that a hydrogen shell flash will not occur at advanced stages of evolution (see below). We want to stress that while the buffer mass is extremely small when departure from AGB takes place during quiescent helium burning, the burning of all excess hydrogen in the red prevents the existence of helium buffer masses as low as $\approx 0.001\,M_\odot$ from occurring. This inhibits the occurrence of diffusion-induced hydrogen shell flashes during the white dwarf phase. We speculate that small helium buffer masses at the start of the cooling branch could be possible only in cases when the progenitor leaves the AGB during the helium shell flash at the surface luminosity peak or during the early portion of the stationary hydrogen burning phase. We plan to place this speculation on a more quantitative basis in a future work. Finally, we want to mention that the total helium content within the star

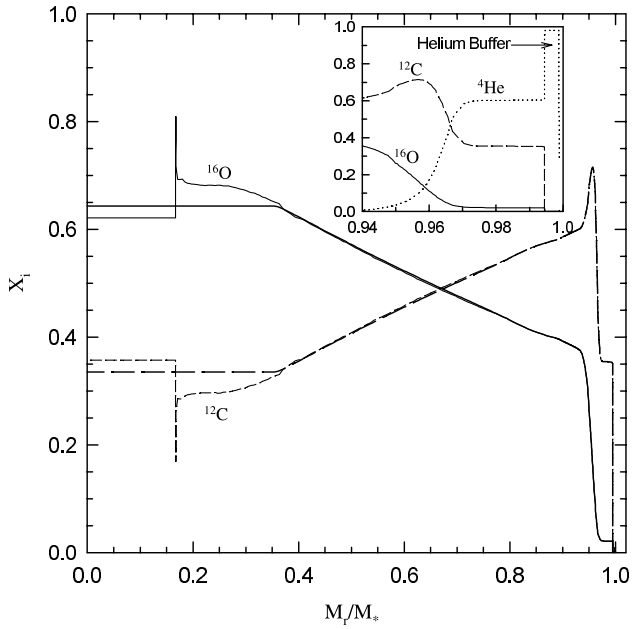

Figure 5. Carbon and oxygen abundance profiles in the core of the 0.563-$M_\odot$ remnant for a progenitor with initially 3 $M_\odot$ shortly after the end of mass loss episodes. Thick lines depict the profile after the chemical rehomogenization caused by Rayleigh–Taylor instability has occurred in the central region of the star, whilst thin lines correspond to the situation before the occurrence of such a rehomogenization. The inset shows the abundance distribution for carbon, oxygen and helium in the outer layers.

[3] Should departure have occurred very late in the pulse cycle, then a last helium shell flash would be expected to occur in the planetary nebula nuclei stage or even in the white dwarf regime, thus giving rise to a born-again AGB star (Schönberner 1979; Iben 1984).

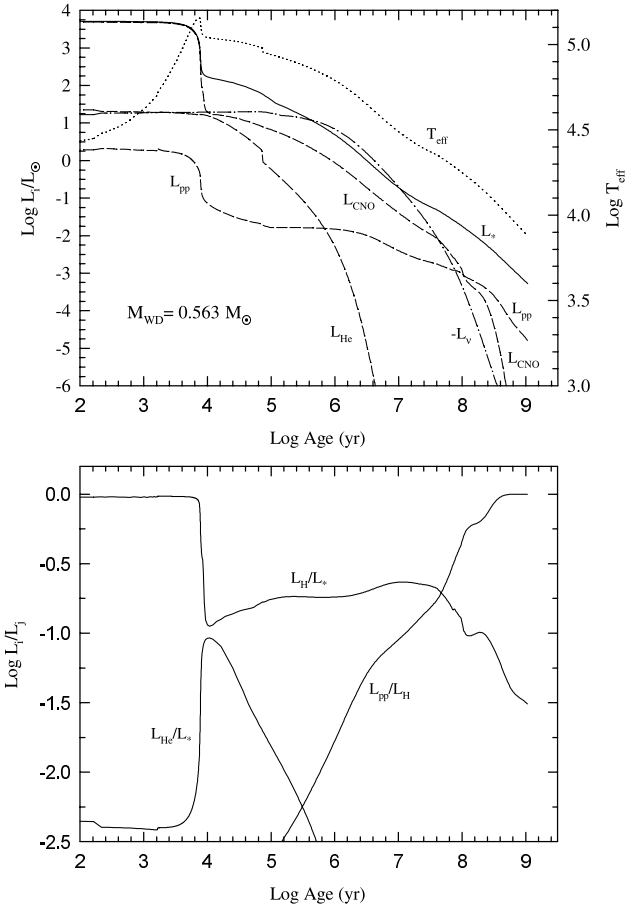

Figure 6. The top panel plots different luminosity contributions (in solar units) as a function of time for the 0.563-$M_\odot$ white dwarf remnant: surface luminosity, L_*, luminosity caused by proton–proton reactions, L_{pp}, CNO bi-cycle, L_{CNO}, helium burning, L_{He}, and neutrino losses, L_ν. The evolution of the effective temperature is also plotted. Here, the zero-age point corresponds to the moment when the model reaches the point defined by $\log L/L_\odot = 3.71$ and $\log T_{eff} = 4.40$. The bottom panel displays luminosity ratios. L_H denotes the complete luminosity as given by hydrogen burning ($L_H = L_{CNO} + L_{pp}$). Note that by the time the ZZ Ceti domain is reached, hydrogen burning, which is almost entirely caused by proton–proton reactions, attains a local maximum, providing a contribution to the surface luminosity output of ~10 per cent. Time is in yr.

once helium shell burning is eventually extinguished remains $0.014\,M_\odot$.

The time dependence of the luminosity contribution caused by hydrogen burning via proton–proton reactions (L_{pp}) and CNO bi-cycle (L_{CNO}), helium burning (L_{He}), and neutrino losses (L_ν), and the surface luminosity (L_*) for the 0.563-$M_\odot$ white dwarf remnant is shown in the upper panel of Fig. 6 from evolutionary stages corresponding to the planetary nebula nuclei down to the lowest computed surface luminosities. Luminosities are in solar units, and the age is counted in years from the moment the model reaches the point defined by $\log L/L_\odot = 3.71$ and $\log T_{eff} = 4.40$. The relative contribution of hydrogen ($L_H = L_{CNO} + L_{pp}$) and helium burning to surface luminosity is displayed in the lower panel of Fig. 6. In addition, the ratio L_{pp}/L_H is shown. Some features of Fig. 6 deserve comment. To begin with, note that at early times nuclear burning via the CN cycle mostly contributes to the surface luminosity of the star. After 7×10^3 yr of evolution (that is shortly after the remnant reaches the maximum effective temperature), the CN cycle reactions abruptly cease, and the model begins to descend to the white dwarf domain and the surface luminosity of the star begins to decline steeply. At these stages, helium burning contributes almost as much to surface luminosity as hydrogen burning. Thereafter, nuclear burning plays a minor role in the evolution of the star, which is dictated essentially by neutrino losses and the release of gravothermal energy. The maximum contribution of nuclear burning to surface luminosity during the white dwarf regime occurs in the effective temperature range of 35000–20000 K (at 5×10^6 to 4×10^7 yr) of evolution. During this phase of evolution, nuclear burning is due almost entirely to CN cycle reactions at the base of the hydrogen layer. These results agree quantitatively with those of Iben & MacDonald (1986) in the frame of 0.6-$M_\odot$ white dwarf models with time-dependent diffusion and $Z = 0.02$. At an age of $\approx 10^8$ yr, the energy production caused by CN cycle reactions falls below that caused by the proton–proton chain and by the time the white dwarf has reached the domain of the ZZ Ceti instability strip, the nuclear energy production is almost entirely from the proton–proton chain. During this stage, the ratio of nuclear-to-surface luminosity reaches a local maximum. Note that at the hot edge of the ZZ Ceti region, nuclear burning contributes at most 10 per cent to the surface luminosity output, and this reduces to 5 per cent when the red edge is reached. Eventually, hydrogen burning becomes virtually extinct at the lowest luminosities that we compute.

Once the remnant has settled upon its cooling track, its chemical abundance distribution will be strongly modified by the various diffusion processes acting during white dwarf evolution. To illustrate this important aspect, we plot in Fig. 7 the abundances by mass of ^{1}H, ^{3}He, ^{4}He, ^{12}C and ^{14}N as a function of the outer mass fraction q ($q = 1 - M_r/M_*$, so the centre of the star corresponds to $\log q = 0$) at various epochs characterized by values of $\log L/L_\odot$ and $\log T_{eff}$ (numbers given in parentheses). In addition, the nuclear energy release ϵ_{nuc} (in erg g^{-1} s^{-1}) caused by hydrogen and helium burning shells are shown as thin lines. Fig. 7(a) shows the chemical stratification before the star reaches the point of maximum effective temperature at high luminosities. In the outermost layers, abundances correspond essentially to those assumed for the interstellar medium. The deeper layers in the helium buffer zone show a CNO abundance that is different from the interstellar one, because hydrogen burning in earlier evolutionary phases processed essentially all the initial ^{12}C into ^{14}N. Fig. 7(b) depicts the situation somewhat later when the star is at the start of the cooling branch 5×10^5 yr after mass loss stops. During these evolutionary stages diffusion is barely noticeable except for the outermost layers where gravitational settling causes hydrogen to float to the surface and heavier elements to sink down. During this part of evolution, the chemical composition changes primarily as a result of nuclear burning via the CN cycle at the base of the hydrogen envelope. With further cooling (Figs 7c and d), the action of gravitational settling and chemical diffusion is apparent. The effect of chemical diffusion is clearly seen at the chemical interfaces where large abundance gradients exist. As a result, in the helium buffer there is a tail of the hydrogen and, at advanced stages, a tail of carbon from the bottom. The tail of hydrogen chemically diffusing inwards to hotter layers (thus favouring the occurrence of hydrogen burning, see below) is clearly noticeable in these figures, as well as the gravitational settling of heavy elements from the outer layers. The chemical stratification when the model reaches the domain of the ZZ Ceti after 3×10^8 yr is displayed in Fig. 7(e). Needless to say, diffusion processes have substantially altered the chemical abundance distribution within the star compared with the initial

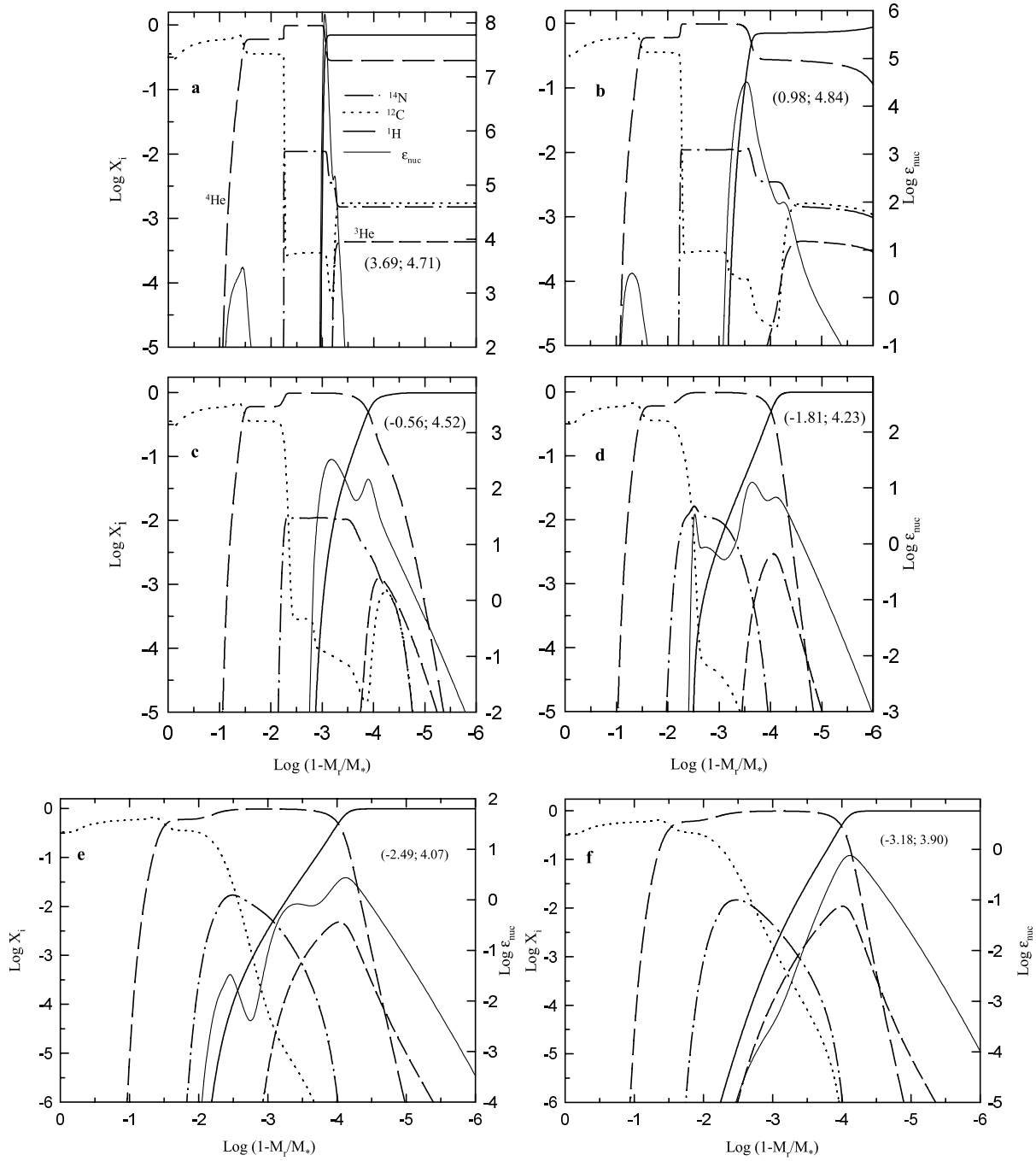

Figure 7. Abundance by mass of ^{1}H, ^{3}He, ^{4}He, ^{12}C and ^{14}N as a function the outer mass fraction for the 0.563-$M_\odot$ white dwarf remnant at selected evolutionary stages characterized by values of $\log L/L_\odot$ and $\log T_{\rm eff}$ (numbers given in parentheses). In addition, the nuclear energy release $\epsilon_{\rm nuc}$ (in erg g^{-1} s^{-1}) caused by hydrogen and helium burning is shown as thin lines (the latter of some relevance only in parts a and b). The model displayed in (a) corresponds to the evolutionary stage before reaching the point of maximum effective temperature at high luminosities, whilst the model plotted in (f) corresponds to the last computed model. Part (e) depicts the situation in the ZZ Ceti domain. For this model, note both the inward extent of the tail in the hydrogen distribution caused by chemical diffusion and the large mass range over which hydrogen nuclear burning extends. Clearly, element diffusion substantially alters the chemical abundance distribution during the white dwarf evolution.

stratification at the start of the cooling branch. In particular, the star is characterized by a pure hydrogen envelope of mass $3.5 \times 10^{-5}\,M_\odot$ plus a wide tail of hydrogen reaching very deep layers (by this time, the total hydrogen content left in the star amounts to $7 \times 10^{-5}\,M_\odot$). Indeed, the tail of the hydrogen distribution reaches a maximum depth by this epoch. Note also the tail of carbon diffusing into the helium buffer from deeper layers. With further cooling, the diffusive tail of hydrogen begins to retreat outwards again, because the increasing electron degeneracy causes chemical diffusion to become less important and the inward diffusion of hydrogen is stopped. The chemical profile corresponding to the last computed model is shown in Fig. 7(f). It is clear that, except for the outermost layers at large ages, the situation of diffusive equilibrium has not been reached even at the latest evolutionary

stages we computed. So, the diffusive equilibrium approach used to infer the chemical profile of DA white dwarfs in some pulsation studies of these stars is not entirely appropriate. Another interesting observation concerning the importance of diffusion in the element distribution is related to the evolution of ^{12}C and ^{14}N abundances in the buffer layer. Indeed, initially the ^{14}N abundance in the helium buffer overwhelms that of ^{12}C (see Fig. 7a), but at the latest stages computed, ^{14}N is less abundant than ^{12}C in almost all the stellar interior, despite the fact that nuclear burning has processed considerable ^{12}C into ^{14}N during white dwarf evolution. The same finding has been reported by Iben & MacDonald (1986), although in their calculations, the ^{12}C abundance exceeds the ^{14}N abundance by the time the ZZ Ceti domain is reached. This is earlier than takes place in our calculation. In part, this difference between the two sets of calculations can be understood on the basis that in the present study we have included thermal diffusion, whilst this process has been neglected by Iben & MacDonald (1986). Because thermal diffusion acts in the same direction as that of gravitational settling, the neglect of the former leads to a larger ^{12}C abundance in the helium buffer. In this context, this effect is expected to be responsible for differences in the nuclear burning luminosity as compared with the situation in which thermal diffusion is considered. To verify these assertions, we have computed the white dwarf evolution of the remnant but without considering thermal diffusion. In fact, we found that in such a case the resulting ^{12}C abundance by the time the ZZ Ceti domain is reached becomes somewhat larger at the tail of its distribution; in addition, the contribution of nuclear burning to surface luminosity increases (by at most 20 per cent) when thermal diffusion is not taken into account.

An aspect worthy of discussion is the effect that chemical element diffusion has on nuclear burning. This important point has been studied in detail by Iben & MacDonald (1985) in the case of models with $Z = 0.001$. The situation for the case $Z = 0.02$ is qualitatively similar though some differences exist. In broad outline, diffusion causes CN cycle reactions to be efficient for a longer period of time than when diffusion is neglected. This can be understood by inspecting the distribution of nuclear energy generated within the star given in Fig. 7. Indeed, as a result of hydrogen diffusing downwards to hotter layers into the helium buffer and carbon diffusing upwards from the carbon-rich zone through the buffer layer, the production of nuclear energy via CN cycle reactions remains significant for a long period of time in the white dwarf evolution. The location of the peak in $\epsilon_{\rm CN}$ becomes deeper as evolution proceeds, reaching a maximum depth at a mass of $\approx 1.7 \times 10^{-3}\,{\rm M}_{\odot}$ below the stellar surface. Note that despite chemical diffusion leading to appreciable abundances of ^{1}H and ^{12}C in the helium buffer, this has not resulted in an enhanced nuclear energy release. However, this could have been radically different had the helium buffer been less massive than ours ($\approx 0.003\,{\rm M}_{\odot}$). In fact, Iben & MacDonald (1986) showed that a hydrogen shell flash is initiated when the star has already settled upon the white dwarf cooling track if the helium buffer mass is as small as $0.001\,{\rm M}_{\odot}$, and that the thermonuclear runaway is avoided if it is as massive as $0.005\,{\rm M}_{\odot}$. As mentioned earlier, how massive the helium buffer can be depends (for a progenitor of a given initial stellar mass) on the precise phase in the helium shell flash cycle at which the star departs from the AGB. So, the role played by the CN cycle reactions in producing nuclear energy during the white dwarf stage will also depend on the phase of the helium shell flash cycle at which departure from the AGB occurs. Finally, we note that as cooling proceeds, the mass range over which hydrogen nuclear burning extends becomes wider as fast as the tail of the hydrogen distribution penetrates inwards. As can be seen, the maximum width is found at the ZZ Ceti region, so in principle the mode stability in DA white dwarf models could be affected by the occurrence of nuclear burning over a considerable mass range. In this connection, it is worth commenting on the fact that shell nuclear burning has been found to be responsible for the instability of g-modes through the ϵ-mechanism in models of pre-white dwarfs (see Kawaler et al. 1986; Kawaler 1988). However, the periods of the excited modes are so short that they have not been observed in such stars (Hine & Nather 1987). Anyway, we find that hydrogen burning contributes at most 10 per cent to surface luminosity during the ZZ Ceti stage. We want to stress that according to our calculations nuclear burning during the white dwarf stage does not represent a major source of energy even for the maximum hydrogen mass allowed by the pre-white dwarf evolution. This is a consequence not only of the fact that in this calculation we assume a high initial metallicity ($Z = 0.02$) (see Iben & MacDonald 1986) but also that, as mentioned, the inclusion of the thermal diffusion process lessens the hydrogen burning contribution to surface luminosity.

Because the shape of the chemical composition profile is a key factor in determining the g-mode periods of DAV white dwarfs, we compare in Fig. 8 the chemical stratification of the white dwarf at the instability domain (thick lines) with that corresponding at the start of the cooling branch (thin lines). The role of diffusion is again clearly emphasized in this figure. Notably, near-discontinuities in the initial abundance distribution are smoothed out considerably by element diffusion. In fact, diffusion processes strongly modify the slope of the chemical profiles in the outer

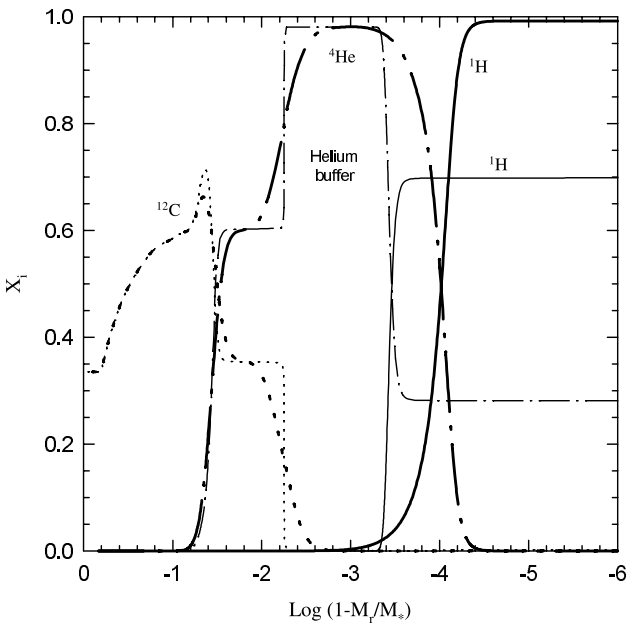

Figure 8. Abundance profiles for our 0.563-$M_{\odot}$ white dwarf remnant for two selected models just after the maximum effective temperature point (model with thin lines) and near the beginning of the ZZ Ceti regime. The models are characterized by values ($\log L/L_{\odot}$, $\log T_{\rm eff}$) of (3.1, 5.15) and (-2.48, 4.07) (thin and thick lines, respectively). In particular, the distribution of hydrogen, helium and carbon (solid, dot-dashed and dotted lines, respectively) is depicted as a function of the outer mass fraction. The importance of element diffusion in the distribution of chemical abundance is clearly noticeable.

layers on the white dwarf cooling track. As is well known, such regions are critical for the pulsation properties of white dwarfs. In the next section, we describe the effect of such chemical profiles on the main quantities entering adiabatic pulsation equations.

In what follows, we shall comment on the implications of the results we have discussed thus far for those quantities entering the pulsation equations that depend essentially on the profile of the chemical composition. Here, we shall limit ourselves exclusively to that aspect, deferring a thorough discussion of the consequences for the global pulsation properties of the model to a future work.

4 QUANTITIES FOR ADIABATIC PULSATION ANALYSIS

Here we describe at some length the characteristics of the basic variables that are relevant for adiabatic pulsation analysis. We shall concentrate particularly on the Brunt–Väisälä frequency (hereafter BVF) and the Ledoux term (B). To perform our analysis, we pick out a model within the ZZ Ceti instability strip ($T_{\rm eff} \sim 12\,000$ K).

Roughly speaking, the BVF is the oscillation frequency of a parcel of stratified stellar fluid when it is vertically (radially) displaced from its equilibrium level, and buoyancy acts as restoring force. The BVF (N) is defined as (Unno et al. 1989):

$$N^2 \equiv g\left(\frac{1}{\Gamma_1}\frac{{\rm d}\ln P}{{\rm d}r} - \frac{{\rm d}\ln \rho}{{\rm d}r}\right). \tag{1}$$

As is well known, the shape of the BVF is directly responsible for the global characteristics of the period spectrum in pulsating white dwarfs. It can be demonstrated by employing a local analysis (see, e.g., Unno et al. 1989) that the condition for propagating (non-evanescent) g-modes is that the frequency squared, σ^2, must be less than both L_ℓ^2 and N^2, where L_ℓ is the (acoustic) Lamb frequency (the other critical frequency of non-radial stellar oscillations). The region of the model where this condition is accomplished is the propagation zone of the mode (see propagation diagrams in, for example, Cox 1980; Unno et al. 1989). In particular, for white dwarfs, the BVF reaches very small values deep in the degenerate core, thus excluding the possibility for propagation of low-order g-modes (short periods). Instead, these modes propagate in the envelope of the star, and are therefore very sensitive to the detailed structure of the outer regions.

From the computational point of view, the treatment of the BVF in the interior of white dwarf stars has been thoroughly discussed previously (see Tassoul et al. 1990, and in particular Brassard et al. 1991). These studies illustrate the numerical problems and systematic errors that result from the computation of the BVF when it is assessed directly from its definition (equation 1). Brassard et al. (1991) have shown that, in the frame of their stellar models, the profile of BVF obtained from equation (1) can lead to an unreliable pattern of g-mode periods. As pointed out in that article, the reason for that is not the computing of the numerical derivatives themselves, but instead, that the direct employment of equation (1) for strongly degenerate matter typical of white dwarf interiors implies subtracting two large quantities that are nearly equal, which produces, besides spurious structures in the N profile, a global shift towards greater BFV values, particularly in the inner core [see this notable effect in fig. 10a of Brassard et al. (1991)]. This leads to an increase in the eigenfrequencies of g-modes, or, in other words, to a displacement towards shorter periods. In addition, the region of period formation, as sketched from the weight functions (see Brassard et al. 1991), is strongly affected.

To overcome these difficulties, Brassard et al. (1991) provide a computational strategy appropriate for degenerate objects, known in the literature as a 'modified Ledoux' treatment. According to these authors, N^2 in white dwarf models is to be computed as

$$N^2 = \frac{g^2\rho}{P}\frac{\chi_{\rm T}}{\chi_\rho}(\nabla_{\rm ad} - \nabla + B), \tag{2}$$

where $\chi_{\rm T}$ (χ_ρ) denotes the partial logarithmic pressure derivative with respect to T (ρ), ∇ and $\nabla_{\rm ad}$ are the actual and adiabatic temperature gradients, respectively, and B, the Ledoux term, is given by

$$B = -\frac{1}{\chi_{\rm T}}\sum_{i=1}^{n-1}\chi_{X_i}\frac{{\rm d}\ln X_i}{{\rm d}\ln P}. \tag{3}$$

where X_i is the abundance by mass of species i, n is the total number of considered species and

$$\chi_{X_i} = \left(\frac{\partial \ln P}{\partial \ln X_i}\right)_{\rho,T,\{X_{j\neq i}\}}. \tag{4}$$

This formulation has the advantage of avoiding the problems mentioned above, and at the same time it explicitly accounts for the contribution to N^2 from any change in composition in the interior of model (the zones of chemical transition) by means of the Ledoux term (equation 3). Brassard et al. (1992a) stress the relevancy of a correct treatment of the BVF in the interfaces of chemical composition in stratified white dwarfs, particularly in connection with the resonance effect of modes known as 'mode trapping'. The modified Ledoux treatment is employed in most of the pulsation studies in white dwarfs.[4] Our pulsation code (Córsico & Benvenuto 2001) is also based on such a formulation.

The Ledoux term B is an important ingredient in the computation of N^2. In most existing studies, the shape of B is computed from chemical profiles treated on the basis of diffusive equilibrium in the trace element approximation (see, for example, Tassoul et al. 1990; Brassard et al. 1991, 1992a,b). The behaviour of B is responsible (through N^2) for macroscopic effects on the period distribution in stratified white dwarfs, such as the mode trapping and mode confinement (in the terminology of Brassard et al. 1992b). In the upper panel of Fig. 9 we show the profiles of abundances for the most relevant chemical species of our models (see Section 3.2). In the centre panel we depict the corresponding B term and in the bottom panel we plot N^2. The chemical profiles as predicted by our calculations are very smooth in the interfaces, which give rise to extended tails in the shape of B. Also, note that our model is characterized by a chemical interface in which three ionic species coexist in appreciable abundances: oxygen, carbon and helium. This transition gives two contributions to B, one of them of relatively great magnitude, placed at $\log q \sim -1.4$, and the other, more external and of very low height at $\log q \sim -2.2$. This feature makes a difference compared with the results of other authors (see Tassoul et al. 1990; Brassard et al. 1991, 1992a,b; Bradley 1996). As a last remark, we note that the contribution of the He–H interface to B is less than that corresponding to the O–C–He transition. From the bottom panel of Fig. 9 we can note each feature of B reflected in the shape of the BVF. The contributions of the Ledoux term are translated into extended bumps on N^2. Note the global smooth behaviour of these quantities when account is made of evolutionary models with time-dependent

[4] Except, for example, in Gautschy et al. (1996).

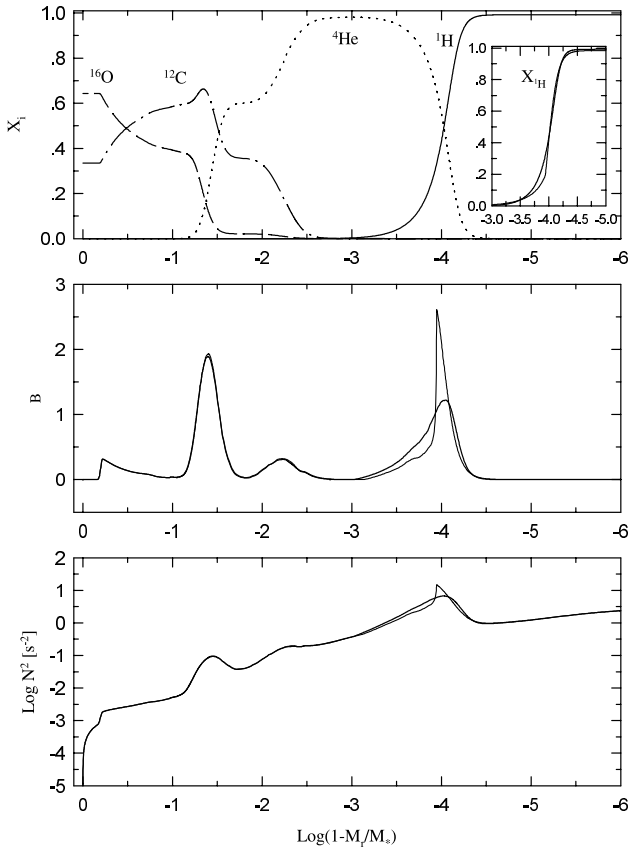

Figure 9. Upper panel: the internal chemical profiles for a ZZ Ceti model of $0.563\,M_\odot$ at $T_{\rm eff} = 12\,000$ K, for hydrogen (solid line), helium (dotted line), carbon (dot-dashed line) and oxygen (dashed line). The inset shows the chemical profile at the hydrogen–helium interface together with the prediction of the diffusive equilibrium in the trace element approximation, as given by the thin line. Centre panel: the corresponding Ledoux term B. The thin line depicts the results for the diffusive equilibrium approximation. Bottom panel: the logarithm of the squared Brunt–Väisälä frequency. The thin line corresponds to the case of the diffusive equilibrium approximation.

element diffusion. In the interests of comparison, we have also computed B and N^2 according to the prediction of the diffusive equilibrium in the trace element approximation as given by Tassoul et al. (1990). The resulting chemical profile at the hydrogen–helium transition as given by this approximation is depicted by thin lines in the inset of the upper panel of Fig. 9. In agreement with previous studies, note that the equilibrium diffusion approximation leads to a pronounced peak in the Ledoux term at that chemical interface, which translates into a sharp peak of N^2 in that region.

For the sake of completeness, we have also computed N^2 from equation (1). After some minor manipulations, and using the hydrostatic equilibrium condition ($\mathrm{d}P/\mathrm{d}r = -\rho g$), equation (1) can be rewritten as

$$N^2 = -\frac{g^2\rho}{P}\left(\frac{\mathrm{d}\ln\rho}{\mathrm{d}\ln P} - \frac{1}{\Gamma_1}\right). \qquad (5)$$

The derivative $\mathrm{d}\ln\rho/\mathrm{d}\ln P$ in equation (5) has been computed numerically employing an appropriate interpolation scheme. This scheme provides the first derivative for the interpolated points. The result for N^2 is shown in Fig. 10(a) in terms of r/R_*. In the interests of comparison, Fig. 10(b) shows N^2 computed using the modified Ledoux treatment, from equation (2). Note that our strategy for the

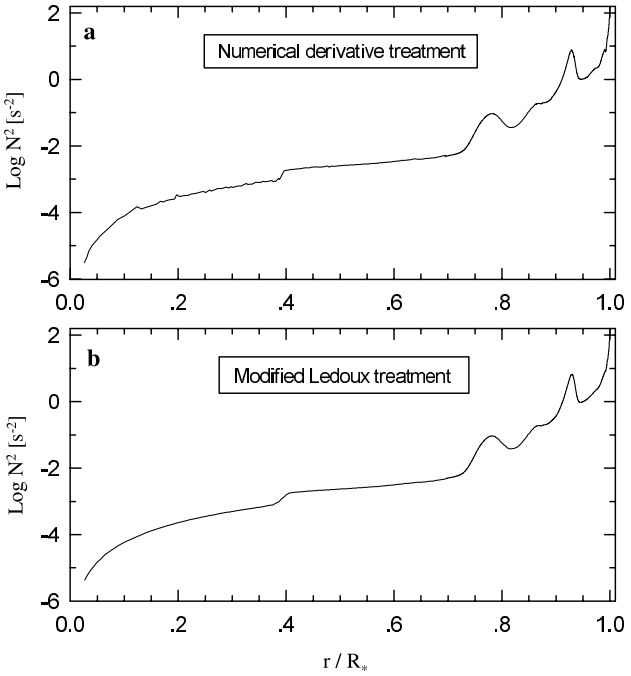

Figure 10. (a) The logarithm of the squared Brunt–Väisälä frequency as a function of the stellar radius computed using numerical derivatives in equation (5). (b) The same quantity but computed from equation (2). The stellar model is the same as that of Fig. 9.

numerical derivatives gives excellent results, reproducing rigorously to the finest detail of the N^2 profile as computed from equation (2). Very small structures (numerical noise) towards the centre can barely be observed. Clearly, in contrast to the assertions of Brassard et al. (1991), our calculations based on an appropriate scheme of interpolating, provides a reliable profile for N^2 in our stellar models (see also a similar finding in Gautschy et al. 1996).

5 CONCLUSION

In this work we present new evolutionary calculations for DA white dwarf stars. The calculations fully take into account time-dependent element diffusion, nuclear burning and the history of the white dwarf progenitor in a self-consistent way. The primary application of our evolutionary models will be the exploration of their pulsation properties in future papers. Evolutionary calculations are carried out by means of a detailed and up-to-date evolutionary code developed by us at La Plata Observatory. The code has been employed in prior studies of white dwarf evolution and it has recently been substantially modified to study the evolutionary stages previous to the formation of white dwarfs. Briefly, up-to-date OPAL radiative opacities for different metallicities, conductive opacities, neutrino emission rates and equation of state are considered. In addition, we include a network of 30 thermonuclear reaction rates for hydrogen and helium burning and the evolution of 13 chemical species resulting from nuclear burning is followed via an implicit method of integration. Our code enables us to also compute the evolution of the chemical abundance distribution caused by the processes of gravitational settling, thermal and chemical diffusion. The treatment for time-dependent diffusion is based on the formulation of multicomponent gases by Burgers (1969).

Specifically, we follow the evolution of an initially 3-$M_\odot$ model

from the ZAMS (the adopted metallicity is 0.02) all the way from the stages of hydrogen and helium burning in the core up to the thermally pulsing phase at the tip of the AGB. By the end of core helium burning, the star experiences a total of 40 micropulses of low surface luminosity amplitude. Afterwards, evolution proceeds to the phase of major thermal pulses on the AGB, during which helium shell burning becomes unstable (helium shell flashes). After experiencing 11 thermal pulses, the model is forced to evolve towards its white dwarf configuration by invoking strong mass loss episodes. Evolution is pursued until the domain of the ZZ Ceti stars on the white dwarf cooling branch.

We find that if departure from the AGB occurs early in the interflash cycle during stationary helium burning, then, after the end of mass loss episodes (at $\log T_{\rm eff} = 3.8$), the star returns to the red where, in the meantime, the hydrogen mass is considerably reduced by hydrogen shell burning over a long period of time. As a result, no planetary nebula is produced. Indeed, the remnant needs $\sim$48 000 yr to reach an effective temperature of 30 000 K required for the excitation of the nebula. This is in agreement with previous full evolutionary calculations of post-AGB stars by Mazzitelli & D'Antona (1986) and Wood & Faulkner (1986). The mass of hydrogen that is left at the start of the white dwarf cooling branch is $\sim 1.5 \times 10^{-4}\,{\rm M}_\odot$, and this is reduced to $7 \times 10^{-5}\,{\rm M}_\odot$ owing to the interplay of further nuclear burning and element diffusion by the time the ZZ Ceti domain is reached. Because we have not invoked additional mass loss episodes during the planetary nebula stage or early during the cooling branch, the quoted value for the final hydrogen mass should be considered as an upper limit. Another feature of interest shown by our results is related to the mass of the helium buffer. We find that when the progenitor leaves the AGB, the helium buffer mass is $\approx 3 \times 10^{-4}\,{\rm M}_\odot$, but as the remnant returns to the red, the buffer mass increases to $0.0024\,{\rm M}_\odot$, which is massive enough to prevent a diffusion-induced hydrogen shell flash from occurring on the white dwarf cooling track. Thus, we conclude that if departure from the AGB takes place during the quiescent helium burning phase, a self-induced nova event as proposed by Iben & MacDonald (1986) is not possible.

In agreement with Iben & MacDonald (1985) we find that element diffusion strongly modifies the distribution of chemical abundances during the white dwarf cooling. Near discontinuities in the abundance distribution at the start of the cooling branch are considerably smoothed out by the diffusion processes by the time the ZZ Ceti domain is reached. Our calculations also show that the situation of diffusive equilibrium has not yet been reached (except for the outermost layers) by the time the ZZ Ceti domain is reached. Indeed, there is an appreciable evolution of the chemical abundances at such stages of evolution. With regard to nuclear burning, we find that it does not represent a major source of energy during the white dwarf stage, as expected for a progenitor star of initially high metallicity. We also find that thermal diffusion lessens even further the importance of nuclear burning.

Finally, we have discussed at some length the implications of our evolutionary models for the main quantities relevant for adiabatic pulsation analysis. We find that the shape of the Ledoux term is markedly different from that found in previous detailed studies of white dwarf pulsations. This is due partly to the effect of smoothness in the chemical distribution caused by element diffusion, which gives rise to less pronounced peaks in the Ledoux term and the Brunt–Väisälä frequency.

We believe that the evolutionary models presented in this work deserve attention concerning their pulsation properties and mode stability. We expect the pulsation properties of our models to show noticeable differences as compared with those encountered in previous studies. Last but not least, fundamental aspects related to the analysis of mode trapping in white dwarfs would be worth carrying out in the frame of the present models. In this sense we speculate that the oscillation kinetic energy of some modes could be considerably affected as a result of the shape of the Brunt–Väisälä frequency as predicted by our evolutionary models. The assessment of such further aspects of white dwarf stars is beyond the scope of the present paper.

Before closing, we would like to comment on the well-known fact that there are still many uncertainties in the theory of stellar evolution that prevent us from being completely confident about the initial chemical stratification of white dwarf stars. For instance, the degree to which semiconvection and overshooting affect the core chemical stratification is not known from first principles, and in most of the studies in which this aspect is addressed they are treated very roughly. In this study overshooting and semiconvection were not included. So, in principle, the profile of the core chemical composition could be somewhat different according to whether these processes are taken into account or not. In addition, the envelope chemical stratification depends quite sensitively on the phase of the helium shell flash cycle at which the progenitor star leaves the AGB. This is particularly true regarding the mass of the helium buffer layer. Finally, mass loss episodes during the planetary nebula stage are expected to reduce the hydrogen envelope mass of the post-AGB remnant. We plan to explore some of these issues and their consequences for pulsation analysis in a future work.

Evolutionary models presented in this paper are available upon request to the authors at their e-mail addresses.

ACKNOWLEDGMENTS

AMS warmly acknowledges Arnold Boothroyd for making available to him the latest set of routines for computing OPAL radiative opacities for different metallicities. It is a pleasure to thank our referee, Paul Bradley, whose comments and suggestions improved the original version of this work.

REFERENCES

Alexander D. R., Ferguson J. W., 1994, ApJ, 437, 879
Althaus L. G., Benvenuto O. G., 1997, ApJ, 477, 313
Althaus L. G., Benvenuto O. G., 2000, MNRAS, 317, 952
Althaus L. G., Serenelli A. M., Benvenuto O. G., 2001a, ApJ, 554, 1110
Althaus L. G., Serenelli A. M., Benvenuto O. G., 2001b, MNRAS, 323, 471
Anders E., Grevesse N., 1989, Geochim. Cosmochim. Acta, 53, 197
Angulo C. et al., 1999, Nucl. Phys. A, 656, 3
Benvenuto O. G., Althaus L. G., 1998, MNRAS, 293, 177
Blöcker T., 1995a, A&A, 297, 727
Blöcker T., 1995b, A&A, 299, 755
Böhm-Vitense E., 1958, Z. Astrophys., 46, 108
Bradley P. A., 1996, ApJ, 468, 350
Bradley P. A., 1998, ApJS, 116, 307
Bradley P. A., 2001, ApJ, 552, 326
Bradley P. A., Winget D. E., 1994, ApJ, 430, 850
Brassard P., Fontaine G., Wesemael F., Kawaler S. D., Tassoul M., 1991, ApJ, 367, 601
Brassard P., Fontaine G., Wesemael F., Hansen C. J., 1992a, ApJS, 80, 369
Brassard P., Fontaine G., Wesemael F., Tassoul M., 1992b, ApJS, 81, 747
Brickhill A. J., 1991, MNRAS, 251, 673
Brown T. M., Gilliland R. L., 1994, ARA&A, 32, 37
Burgers J. M., 1969, Flow Equations for Composite Gases. Academic, New York

Caughlan G. R., Fowler W. A., 1988, At. Data Nucl. Data Tables, 40, 290
Córsico A. H., Benvenuto O. G., 2002, Ap&SS, in press (astro-ph/0104267)
Cox J. P., 1980, Theory of Stellar Pulsations. Princeton Univ. Press, Princeton, NJ
D'Antona F., Mazzitelli I., 1990, ARA&A, 28, 139
Dehner B. T., Kawaler S. D., 1995, ApJ, 445, L141
Dolez N., Vauclair G., 1981, A&A, 102, 375
Gautschy A., Saio H., 1995, ARA&A, 33, 75
Gautschy A., Saio H., 1996, ARA&A, 34, 551
Gautschy A., Ludwig H., Freytag B., 1996, A&A, 311, 493
Goldreich P., Wu Y., 1999, ApJ, 511, 904
Graboske H. C., DeWitt H. E., Grossman A. S., Cooper M. S., 1973, ApJ, 181, 457
Hine B. P., Nather R. E., 1987, in Philip A. G. D., Hayes D. S., Liebert J., eds, Proc. IAU Colloq. 95. The Second Conf. on Faint Blue Stars. L. Davis Press, p. 627
Hubbard W. B., Lampe M., 1969, ApJS, 18, 297
Iben I., Jr, 1982, ApJ, 260, 821
Iben I., Jr, 1984, ApJ, 277, 354
Iben I., Jr, MacDonald J., 1985, ApJ, 296, 540
Iben I., Jr, MacDonald J., 1986, ApJ, 301, 164
Iben I., Jr, Renzini A., 1983, ARA&A, 21, 271
Iben I., Jr, Tutukov A. V., 1984, ApJ, 282, 615
Iglesias C. A., Rogers F. J., 1996, ApJ, 464, 943
Itoh N., Mitake S., Iyetomi H., Ichimaru S., 1983, ApJ, 273, 774
Kawaler S. D., 1988, ApJ, 334, 220
Kawaler S. D., Winget D. E., Hansen C. J., Iben I., Jr, 1986, ApJ, 306, L41
Kaye A. B., Handler G., Krisciunas K., Poretti E., Zerbi F. M., 1999, PASP, 111, 840
Kilkenny D., Koen C., O'Donoghue D., Stobie R. S., 1997, MNRAS, 285, 640
Kippenhahn R., Weigert A., Hofmeister E., , Alder B., Fernbach S., Rottemberg M. 1967, Methods in Computational Physics, Vol. 7. Academic, New York, p. 129
MacDonald J., Hernanz M., José J., 1998, MNRAS, 296, 523
Magni G., Mazzitelli I., 1979, A&A, 72, 134
Mazzitelli I., D'Antona F., 1986, ApJ, 308, 706
Montgomery M. H., Metcalfe T. S., Winget D. E., 2001, ApJ, 548, L53
Salaris M., Domínguez I., García-Berro E., Hernanz M., Isern J., Mochkovitch R., 1997, ApJ, 486, 413
Schönberner D., 1979, A&A, 79, 108
Tassoul M., Fontaine G., Winget D. E., 1990, ApJS, 72, 335
Unglaub K., Bues I., 2000, A&A, 359, 1042
Unno W., Osaki Y., Ando H., Saio H., Shibahashi H., 1989, Nonradial Oscillations of Stars, 2nd edn. Univ. Tokyo Press, Tokyo
Vassiliadis E., Wood P. R., 1993, ApJ, 413, 641
Wallace R. K., Woosley S. E., Weaver T. A., 1982, ApJ, 258, 696
Winget D. E., 1988, in Christensen-Dalsgaard E. J., Frandsen S., eds, Proc. IAU Symp. 123, Advances in Helio- and Asteroseismology. Reidel, Dordrecht, p. 305
Winget D. E., Van Horn H. M., Tassoul M., Hansen C. J., Fontaine G., Carroll B. W., 1982, ApJ, 252, L65
Wood P. R., Faulkner D. J., 1986, ApJ, 307, 659

This paper has been typeset from a TEX/LATEX prepared by the author.